04

Resolving the Spatial Configuration of X-ray Spikes in Magnetoactive Plasma: The July 3, 2017 Solar Flare

© Yu.E. Charikov, V.I. Shuvalova, E.M. Sklyarova, A.N. Shabalin 1,3

¹ loffe Institute.

194021 St. Petersburg, Russia

² Pulkovo Astronomical Observatory, Russian Academy of Sciences,

196140 St. Petersburg, Russia

³ Institute of Space Research, Russian Academy of Sciences,

117997 Moscow, Russia

e-mail: Yuri.Charikov@mail.ioffe.ru

Received May 28, 2024 Revised February 27, 2025 Accepted March 3, 2025

In this study, the spatial distribution of the sources of subsecond bursts (spikes) of hard X-ray radiation was analyzed according to data detected during solar flares by the Konus-Wind, CGRO/BATSE, YOHKOH/HXT, RHESSI, and Fermi GBM spectrometers. An analysis of the temporal structure of hard X-ray emissions from 10 behind-the-limb events revealed spikes in two of them. The SOL2017-07-03T16:13:22 flare (class M1.3) showed spikes in the energy range of 11 to 100 keV during the flux growth stage. The Fermi GBM spectrometer recorded individual spikes with durations of approximately 300–700 ms. The analysis of spatial images of the sources in the EUV lines 171, 94, and 131 Å during this event determined their locations in the upper part of the loop structure of the flare's magnetic field.

Keywords: solar flares, X-rays, EUV, spikes, acceleration.

DOI: 10.61011/TP.2025.07.61446.194-24

Introduction

Despite the growing volume of observational data, the problem of energy release and particle acceleration during solar flares remains one of the unresolved tasks in solar physics. The hard X-ray (HXR) radiation generated by flare-accelerated electrons can potentially reflect the smallest time scales of acceleration processes. In the present study, we analyzed the hyperfine time structure of HXR radiation in flares. The first recording of millisecond X-ray spikes during solar flares was made possible by the launch of the Solar Maximum Mission (SMM) in 1980 and the operation of the Hard X-ray Burst Spectrometer (HXRBS). The HXRBS spectrometer was characterized by its capability of performing relatively fast spectrum measurements and was the first appliance to observe sub-second impulses of an HXR radiation flux of a solar flare [1,2]. In the 1990s, the investigation of the hyperfine time structure of X-ray radiation continued in relation to the launch of the Compton Gamma-Ray Observatory (CGRO) [3]. The full Sun spectrometer Burst And Transient Source Experiment (BATSE) made it possible to perform measurements of the X-ray flux with a high 16-millisecond time resolution, but it could not obtain spatial data on the localization of radiation sources. The similar investigations were performed using data from other spacecraft like SMM [4], Konus-Wind [5] and Fermi [6]. Spatial distribution of X-ray radiation sources was studied using data from the Yohkoh [7] and Reuven Ramaty High

Energy Solar Spectroscopic Imager (RHESSI) [8]. It should be noted that the time structure of flare HXR radiation recorded with a resolution of 16, 64 ms is a non-stationary series with mutually-superimposed separate impulses. In order to reveal separate impulses of ms-duration (hereinafter referred to as "spikes"), a method was proposed, which includes detrending, calculation of a standard deviation as well as criteria of spike determination as a ms-structure of X-ray radiation [9]. X-ray spikes have been recorded in many flares by the full Sun spectrometers [?], but the spatial distribution of the sources of HXR radiation of the spikes is still under investigation. Assuming that the HXR radiation of the spikes is the bremsstrahlung of accelerated electrons, whose efficiency is determined by the densities of the plasma and electron beam, HXR-spike sources should be localized in the chromosphere part of the flare loops, where the plasma density is at least three orders of magnitude higher than in the coronal area of the magnetic loop.

Let us note that the study of the localization of the HXR spikes by the RHESSI spectrometer is difficult due to the necessity of signal demodulation related to tool rotation. As shown in [10], the demodulation process introduces additional systematic uncertainties, thereby limiting the use of RHESSI data for investigating fast time radiation variations. However, analysis of HXR radiation of solar flares recorded in 2002 by the RHESSI spectrometer made it possible for the authors of [11,12] to state that in some flares, the HXR spikes are most likely generated

at the footpoints of the loops located at a distance of 40-50 arc sec apart. The localization of sources in the upper parts of the loops was not revealed in these investigations. We have applied an alternative approach to studying the localization of the HXR spikes based on data obtained by the full Sun spectrometers for the so-called behind-the-limb (partially behind-the-limb) flares, whose loop footpoints (one or both) are occulted for observations from Earth orbit. These observations do not require the application of a complex procedure for demodulating the HXR signal. The high time resolution (16, 64 ms) of the full Sun spectrometers CGRO/BATSE, Konus-Wind, Fermi Gammaray Burst Monitor (Fermi GBM) opens up opportunities for analyzing the hyperfine time structure (spikes) of HXR radiation of the flares. For the behind-the-limb events, it is possible to observe the radiation sources in the upper (coronal) part of the loop structure of the magnetic field, which is visible from the Earth orbit, at the times of appearance (disappearance) at the east or west edges of the Sun disc (limb).

The present study aimed to analyze the millisecond structure of HXR radiation in the coronal parts of the magnetic loops in behind-the-limb flares, whose footpoints (one or both) are hidden from observation from the Earth orbit

It should be noted that the number of recorded behind-the-limb events is small compared to the total number of flares. In accordance with the data of the Konus-Wind catalogue [13], 14 flares were recorded in trigger mode from 2001 to 2015. Nine of them were partly occulted and only 5 of them are behind-the-limb. This is mainly due to the low probability of flares occurring when the tops of loops emerge from the eastern limb or when their lower parts disappear behind the western limb. Before proceeding to the consideration of the structure of HXR radiation of the flares, we discuss the issue of spatial localization of the radiation sources.

It is generally accepted that flare processes occur in active regions (AR), whose structure is determined by the configuration of the magnetic field. For non-limb events, the geometry of the magnetic field in the chromosphere the corona can be obtained in a model of a non-linear force-free field (NLFFF) using the data of measurements from Helioseismic and Magnetic Imager on the satellite Solar Dynamic Observatory (SDO/HMI) as boundary conditions [14,15]. The magnetic field lines, more precisely magnetic flux tubes with a cross-section determined by the scale of magnetic inhomogeneities in the spot, are extended loops of complex geometry with shear. The magnetic flux tubes are filled with plasma, whose parameters differ from the temperature and density of the environment. The loss of stability of such a structure can trigger flares, coronal plasma eruptions, various types of waves, and particle acceleration.It is impossible to directly observe the evolution of the magnetic field; instead, it can be inferred from the variation in the morphology of extreme ultraviolet (EUV) emissions. In the events considered herein, flare EUV radiation at nine

Investigated flares

Flare	X-ray class	Presence of spikes
SOL2002-04-21T01:15:00	X1.5	No
SOL2002-08-03T19:04:05	X1.0	No
SOL2003-10-23T19:54:46	X1.1	No
SOL2004-08-18T17:31:03	X1.8	No
SOL2012-08-06T04:35:40	M1.6	Yes
SOL2013-05-13T02:08:16	X1.7	No
SOL2014-02-25T00:42:44	X4.9	No
SOL2015-03-02T15:25:28	M3.7	No
SOL2015-06-14T00:55:04	M2.0	No
SOL2017-07-03T16:13:22	M1.3	Yes

wavelengths was observed by The Atmospheric Imaging Assembly (SDO/AIA) with a high spatial resolution of $\sim 1\,\mathrm{arc}\,\mathrm{sec}$ and it was a system of loops of different heights with different-temperature plasma. This system of loops was aligned with the configuration of the magnetic field and later matched with discrete sources of HXR radiation. Thus, the X-ray sources were localized relative to the EUV loops and the configuration of the magnetic field.

It should be noted that the loop structure (first of all, its upper part) is seldom observed in X-ray radiation due to the specifics of the deceleration mechanism (bremsstrahlung) of accelerated electrons, which predominantly lose energy in the dense plasma (thick target), i.e. in the chromosphere, and due to the relatively small dynamic range of the X-ray spectrometers. In some events, bright local HXR sources were recorded, spaced apart by at least ten arcseconds [16]. The origin of the third source was attributed to the accumulation of accelerated electrons in the upper part of the structure, which was implicitly associated with EUV loops and, hence, with magnetic loops (arcades) [17]. When comparing HXR sources with EUV maps, it is necessary to consider several causes that prevent strict localization of the HXR source in relation to the EUV loops.

- 1) the lengths of the EUV loops can be comparable with the sizes of the HXR sources;
- 2) there is uncertainty in the co-alignment of EUV and HXR images;
- 3) the question arises as to the validity of comparing localized HXR sources with a continuously emitting EUV loop.

Spatial and temporal structure of HXR emission of the flare SOL2017-07-03

The table lists the partly occulted and behind-the-limb flares, whose hard X-ray emissions were analyzed to reveal

the spike time structure. As shown in the table, no ms structure was detected in approximately 80% of the events.

Let us consider one of the events (see Table), the structure of the HXR radiation in which revealed sub-second impulses. Fig. 1 shows the temporal evolution of solar X-ray emissions recorded by the GOES satellite on July 3, 2017.

The M1.3 class flare was in the active region on the west edge of the solar disc with the coordinates [945,52] arc sec on the 3-d of July, 2017 at 15:54:45 UTC. Solar activity had been low in the preceding days: the background emission did not exceed X-ray class B $(10^{-7} \, \text{W/m}^2)$ in the $(1-8) \, \text{Å}$ range). The last C-class flare was recorded on June 7, 2017. Thus, this AR exhibited virtually no flare activity while crossing the solar disk. Only 9h before the event under study did the activity increase sharply: eight flares occurred, one C1.0 and the others B-class (Fig. 1). These flares can be regarded as preflare indicators of the evolution of the magnetic field.

Fig. 2 shows the time profiles of the X-ray emission from flare SOL2017-07-03, as recorded by FermiGBM. The top panel shows the temporal profile of the flare in four energy channels. The middle panel shows the emission profile in the 26-50 keV channel before detrending, with the trend shown in blue. The bottom panel shows the profile after the detrending. The 4.3–11 keV emission is most likely quasithermal bremsstrahlung from electrons with a Maxwellian velocity distribution, with a possible contribution from lines of highly ionized elements. Its temporal profile shows a monotonic rise, followed by decay. Emission with energies above 25 keV is bremsstrahlung from high-energy electrons. During the first 30 s, the temporal profiles exhibit secondscale pulses, and the peaks of these pulses contain an even finer millisecond-scale structure (spikes). Regarding the emission structure at 11-26 keV, a superposition of quasithermal and bremsstrahlung components is possible.

We will discuss the details of the temporal structure below; for now, we examine the possible spatial localization of the emission sources. Because the AR is located at the solar limb, NLFFF extrapolation of the chromospheric

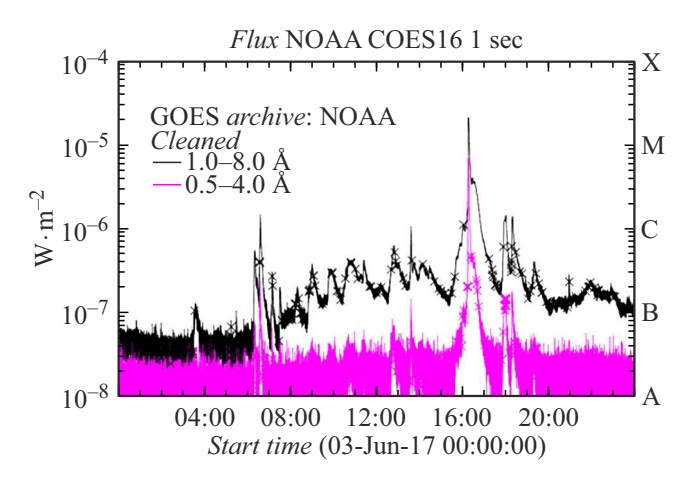


Figure 1. Time history of solar X-ray radiation recorded by the satellite GOES 16 on July 03, 2017

coronal magnetic-field structure is not feasible owing to the lack of SDO/HMI data. This problem can be partly circumvented by using images obtained by the telescope SDO/AIA in nine lines of the EUV range with a high spatial resolution of ~ 1 arcsecond. The EUV images (Fig. 3) obtained by SDO/AIA during the flare in various lines have been analyzed to reveal the system of the loops of both high ones — (20-30) arc sec with the plasma temperature above $10^6\,\mathrm{K}$ as well as low ones (< $10\,\mathrm{arc}\,\mathrm{sec}$), which slowly evolved from the time of recording start at 16:04:06 UTC up to the start of sharp increase of brightness of the low loops at 16:13:18 UTC.

Note that for the 171 Å line, the response function peaks at the Fe IX ionization stage at a temperature of approximately 0.63 MK. In the 131 Å channel, the dominant contributions come from the Fe VIII and Fe XXI lines, which peak at approximately 0.4 and 10 MK, respectively. The interaction of the high-lying loop(s) with the underlying system of loops led to a loss of stability and subsequent ascent (Fig. 3, lower panel, left). It is possible that such a reconfiguration (rise) led to the emergence of a low-lying loop system visible in the EUV lines (Fig. 3 (right panels), which at 16:13:18 UTC was followed by interaction with a pre-existing loop structure, resulting in an abrupt change in the magnetic field configuration. The reconfiguration of the magnetic field facilitated the generation of an inductive electric field, acceleration of electrons to energies up to 100 keV, and their bremsstrahlung X-ray emission. should be taken into account that the RHESSI resolution of 11.8 arc sec (the 4F detector) is much worse than the resolution of SDO/AIA — \sim 1 arc sec. Therefore, when overlaid on EUV images, the areal extent of localized hard X-ray (HXR) sources overlaps them; thus, comparing the images, especially for limb events, does not yield precise co-localization of the sources (Fig. 4). For the SOL2017-07-03 flare, the centroids of the RHESSI X-ray images at 16:13:03 UTC lie essentially at the limb; moreover, the centroids of the 3-6 and 6-12 keV images are slightly displaced upward into the corona (Fig. 5), which most likely correspond to the upper portions of the low-lying magnetic loops visible in the EUV lines (Figs. 4,5). The HXR sources in the 11-26 and 25-50 keV channels are localized somewhat lower, closer to the transition region between the corona and the chromosphere. Numerical kinetic calculations of accelerated-electron transport in flare loops [18] indicate that spikes shorter than 1s cannot be generated in plasma with a density below $\sim 10^{11}\,\mathrm{cm}^{-3}$. An exception is highly anisotropic electron beams; however, their emission would not be observable because the dynamic range of HXR spectrometers is insufficient. Therefore, there is strong evidence that the 11-26 keV source is located in the lower corona, where the plasma density lies in the range from $\sim 10^{11}$ to $\sim 5 \cdot 10^{12} \, \text{cm}^{-3}$. Sources of harder emission (> 50 keV) are located at the limb, at one of the visible EUV loop footpoints. It can be seen that the height distribution of the sources of HXR radiation with different energies does not exceed several arcseconds, which is much

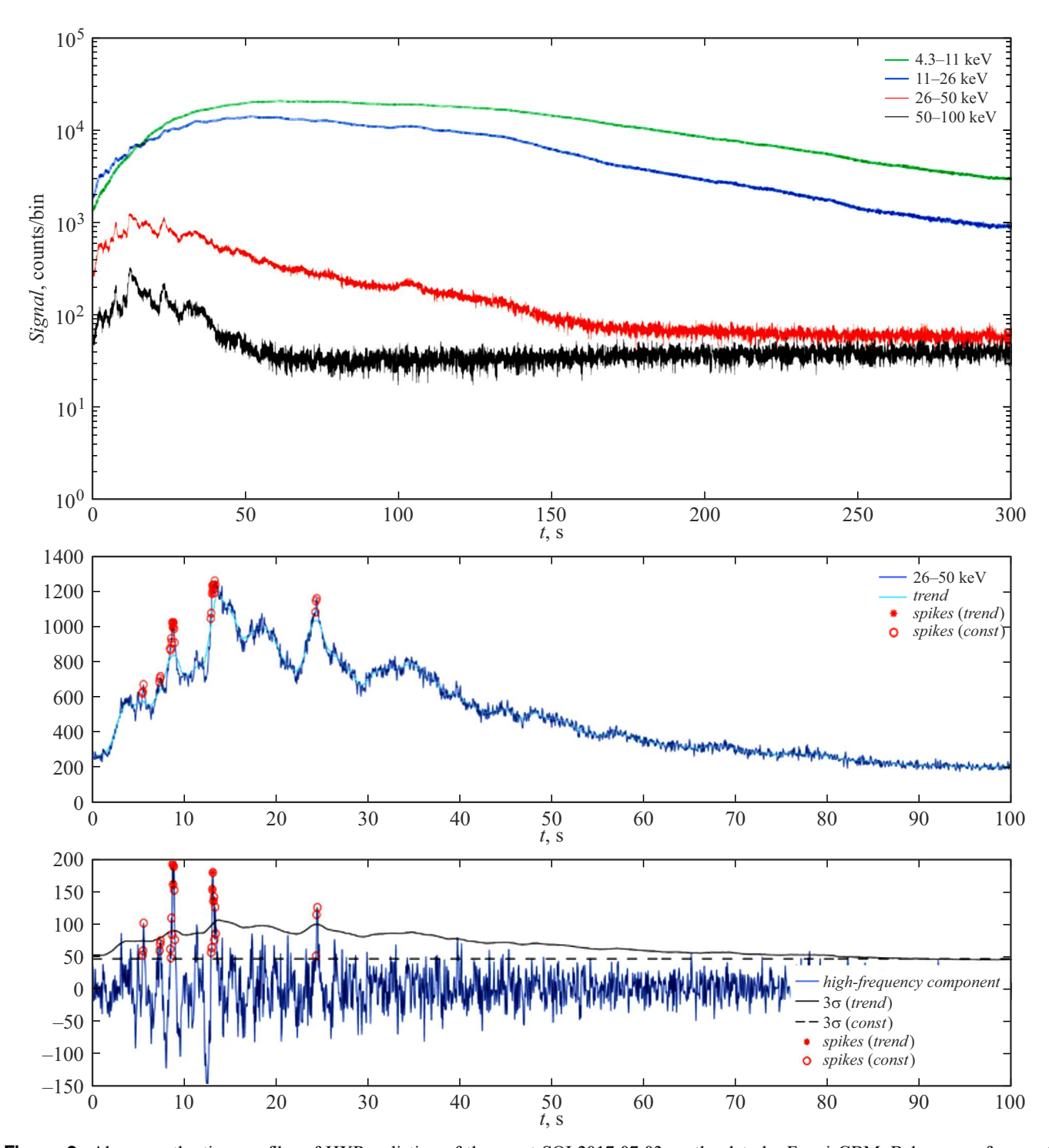


Figure 2. Above — the time profiles of HXR radiation of the event SOL2017-07-03 — the data by Fermi GBM. Below — a fragment of HXR emission $26-50 \,\text{keV}$ with the presence of a trend (the blue curve) and without it. The red markers denote the times of the spike recordings. The time $t=0 \,\text{s}$ corresponds to Universal Time 16:13:18 UTC.

less than the height of visible elevation of the flare loops over the footpoints $\sim (1-3) \cdot 10^9 \, \text{cm} \, (14.3-42.9 \, \text{arc sec})$. Therefore, based on the heights of the HXR sources, this flare can be classified as a partially occulted event.

The explosion phase of the flare started at 16:13:22 UTC and coincided with eruption of plasma visible in the EUV

lines (Fig. 4). A change in the magnetic field configuration most likely caused plasma ejection and triggered the onset of the flare's explosive phase. This conclusion is supported by the observed structural changes in these EUV loops. At the emission peak, the energy spectrum, attributed to bremsstrahlung from accelerated electrons, follows a power

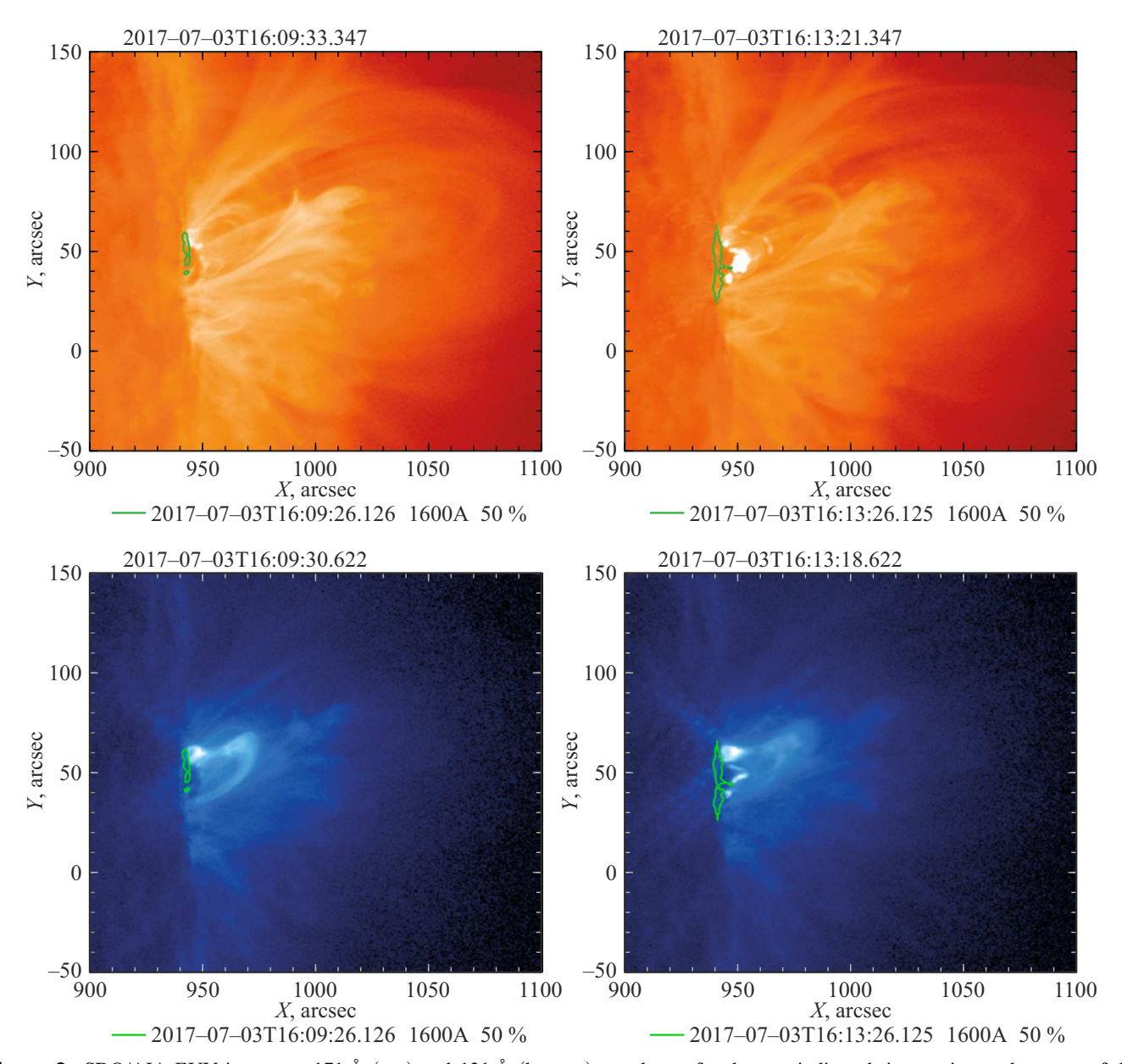


Figure 3. SDO/AIA EUV images at 171,Å (top) and 131,Å (bottom) are shown for the two indicated times prior to the onset of the flare. The green contour corresponds to the $1600 \, \text{Å}$ emission at the $50 \, \%$ level.

law with a spectral index of 3.66 [19] in the 15–100 keV energy range.

Characteristics of HXR Spikes in the SOL2017-07-03 Flare

Millisecond-timescale increases in the count rate (spikes) were observed during the rise and peak phases of the emission (Fig. 2). Let us consider the structure of the separate HXR spikes. First, we discuss the detection of spikes in HXR emission time series. For the flare SOL2017-07-03, the standard deviation σ was determined using several methods:

- (1) as a constant value across the entire high-frequency time series;
- (2) as a variable value equal to the square root of the trend in each time bin;
- (3) as a value calculated using a 30 and 60-second sliding window (Fig. 2).

We emphasize that spikes were detected when the σ level was constant and when it was calculated based on the square root of the trend. The second method for determining the standard deviation appears more robust, as it accounts for the dependence of the noise magnitude on the flare phase. In addition to exceeding the 3σ threshold, a multi-point profile and its repeatability across different energy ranges are important spike selection criteria. Analysis of the HXR profiles (Fig. 6) reveals four spikes in

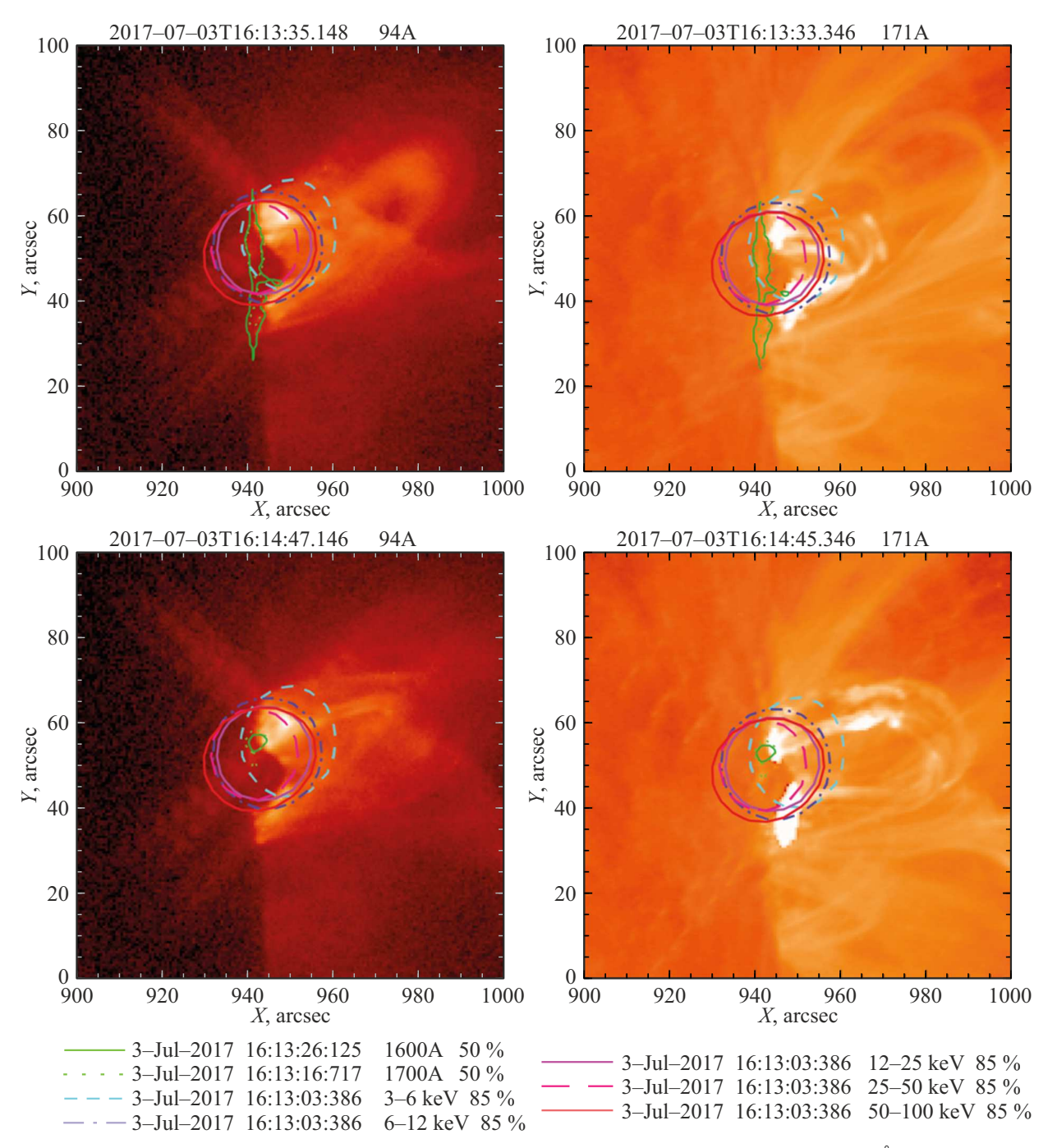


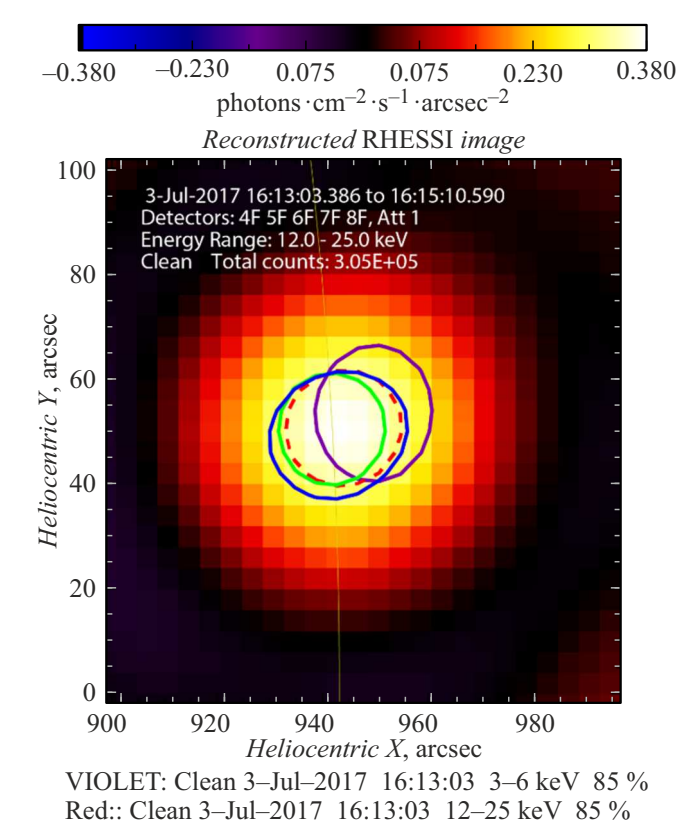
Figure 4. HXR source locations in the SOL2017-07-03 flare (RHESSI data). The EUV images of SDO/AIA 94 Å (left panels) and 171 Å (right panels) are shown at two times (shown above the panels). The contours in the EUV lines 1700 and 1600 Å are shown for the level of 50 %, as are the contours of HXR radiation for the level of 85 %. The HXR contours of all the panels are given for the time, which corresponds to the flare peak.

the specified time interval, although not all of them satisfy all the proposed criteria.

Notably, no spikes were detected in the $4-11 \, \text{keV}$ energy range, which confirms the conclusion of the quasi-thermal emission mechanism. Fig. 6 shows the fragments of the count rates of the flare SOL2017-07-03 within the ranges 11-26, 26-50 and $50-100 \, \text{keV}$, which were recorded in the narrow time interval 16:13:24-16:13:31 UTC by the

Fermi GBM spectrometer. We especially note the similarity of the time profiles of the HXR spikes in the various energy ranges at 16:13:26 UTC, which indicates the similarity of the time profiles of accelerated electrons and the parameters of the flare plasma in the radiation source.

Let us consider the temporal structure of the most pronounced spike in 16:13:26 UTC. Notably, the spike profiles across different energies are symmetric, in contrast



BLUE: Clean 3–Jul–2017 16:13:03 50–100 keV 85 % **Figure 5.** RHESSI HXR image obtained by the Clean method at the energies: 3–6 (violet contour), 12–25 (background and red dashed line), 25–50 (green contour), 50–100 keV (blue contour). The contour lines correspond to the level of 85 %.

GREEN: Clean 3-Jul-2017 16:13:03 25-50 keV 85 %

to the elementary bursts that exhibit a more extended decay phase. The duration of the spikes at the FWHM level is 500–700 ms, while the time resolution (the duration of one bin) is — 0.064 s. Let us pay attention that the time profiles of the spikes in the channels 11-26 (the spectrum weighted mean value of the energy $E_1 = 13.5 \,\text{keV}$, the velocity $v_1 = 6.9 \cdot 10^9 \text{ cm/s}$) and 26-50 ($E_2 = 33.3 \text{ keV}$, the velocity $v_2 = 10.9 \cdot 10^9$ cm/s) (Fig. 6) are similar in the structure and somewhat differ from the profile in the channel 50-100 ($E_3 = 66.6$ keV, the velocity $v_3 = 15.4 \cdot 10^9$ cm/s). We calculated the spectrally weighted mean energy in the low-energy channel ($E_1 = 13.5 \,\mathrm{keV}$) from a powerlaw distribution, neglecting the quasi-thermal contribution. This may lead to a misinterpretation of the actual energy distribution of the electrons that produce this emission. A pairwise cross-correlation analysis of the time lags for the most prominent spike showed that the 50-100 $(E_3 = 66.6 \,\text{keV})$ emission led the $11-26 \,(E_1 = 13.5 \,\text{keV})$ and 25-50 ($E_2 = 33.3 \,\text{keV}$) channels by 77 ms and 9 ms, respectively (Fig. 7). The lag time between the signals was determined by interpolating three points near the maximum of the correlation function by a second-order polynomial (red dashed line, Fig. 7). The time delay spectrum $\tau(E)$

decreases with increasing energy, closely following the $E^{-1/2}$ power law. This behavior is characteristic of the free streaming of accelerated electrons in a magnetic loop.

The validity of the free–streaming model depends on several simultaneous conditions, including co–spatial acceleration and injection, and the subsequent propagation of electrons along the magnetic loop without energy loss or Coulomb scattering. Despite the stringent conditions, the $E^{-1/2}$ law has been approximately observed in many flares [19]. In the SOL2017-07-03 event, the spike emission delays indicate that the $E^{-1/2}$ law is not strictly satisfied. However, the decreasing time delay spectrum suggests that high-energy electrons ($E_3 = 66.6 \,\mathrm{keV}$) radiate first, preceding the lower energy emission by tens of milliseconds.

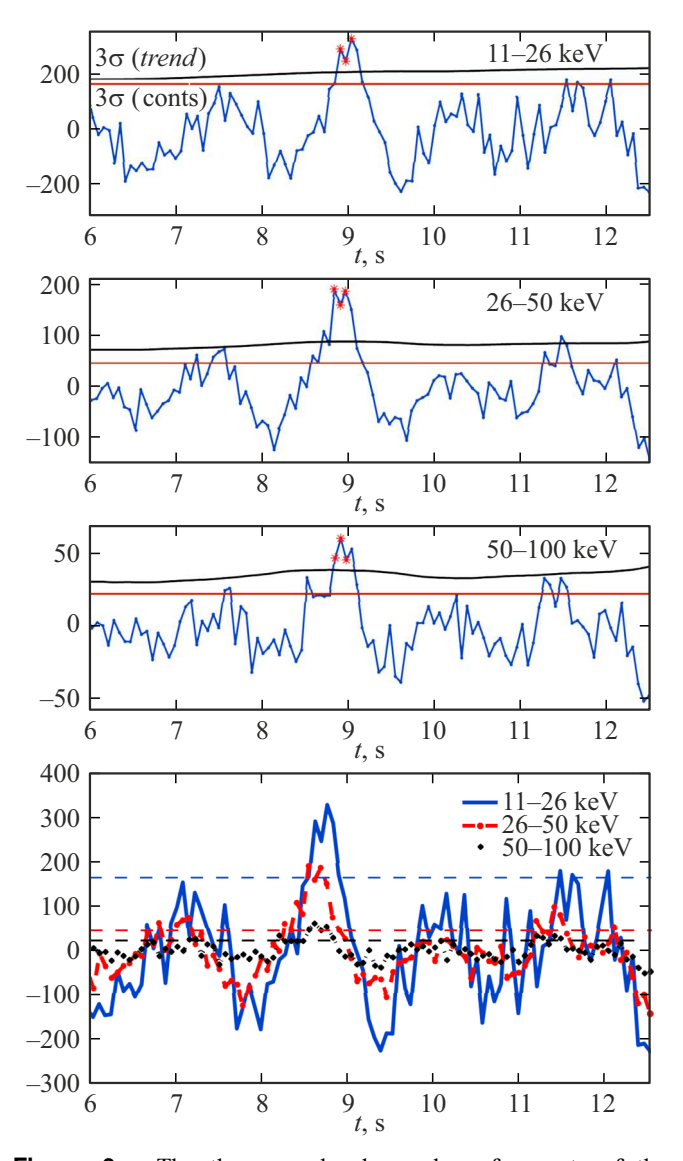


Figure 6. The three panels above show fragments of the count rates of the flare SOL2017-07-03 within the ranges 11–26, 26–50 and 50–100 keV, which are recorded during the time interval 16:13:24–16:13:31 UTC. Below — the same fragments combined into one panel.

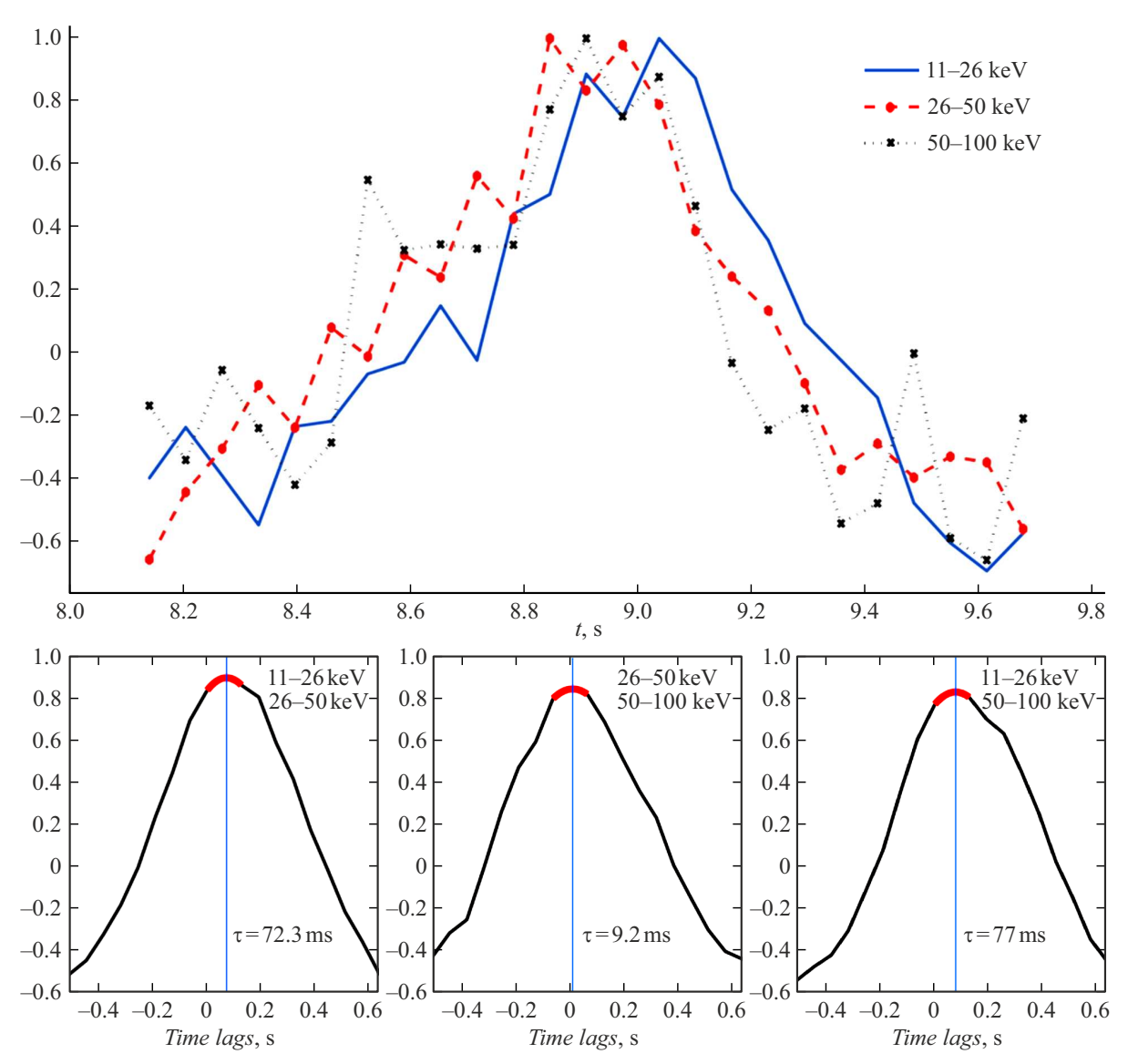


Figure 7. Top: the main spike in the HXR emission of the SOL2017-07-03 flare, with normalized counts in the three energy channels. Bottom: the pairwise correlation functions of the HXR time series.

The observed sub-second delays in X-ray emission must be interpreted with caution, given the statistical uncertainty estimates. As shown in [20,21], the uncertainty in measuring time delays due to noise and photon statistics can be comparable to the instrument's temporal resolution (about 64,ms in our case). Our additional Monte Carlo simulations confirmed these estimates. Thus, while the detected delays align with the expected physical processes of electron acceleration and flare X-ray generation, the potential impact of statistical fluctuations must be considered in the quantitative interpretation of the results.

3. Discussion of the results

Bremsstrahlung X-ray emission is generated most efficiently in the dense plasma of flare loops. The emission measure is proportional to the densities of the plasma and accelerated electron beam. Therefore, we expect the brightest HXR emission sources to be located in the chromospheric parts of flare loops, where the plasma density is at its maximum. While HXR sources can be located at the looptop, they are generally faint because of the lower plasma density relative to the loop footpoints, leading to their less frequent detection. However, as demonstrated above, in the partially occulted flare SOL2017-07-03, the HXR spikes originated not only from the footpoints but also from the tops of a low-lying loop system visible in hot and cool EUV lines. This raises questions about the plasma parameters at the looptop(s) primarily the plasma density and the model for the acceleration and injection of electrons to energies of 100 keV and higher on a millisecond timescale. At the onset of a flare, the plasma density in the looptops is generally no more than

 $10^{10} - 10^{12} \,\mathrm{cm}^{-3}$ [22]. Since the density of $10^{10} \, \text{cm}^{-3}$ is insufficient for the efficient scattering of accelerated electrons on millisecond timescales, an accumulation of both accelerated electrons and thermal protons must occur in the emission source. EUV images of the SOL2017-07-03 flare in multiple channels show that before the HXR spikes in the impulsive phase at 16:13:26 UTC (Fig. 3,4), a loop system had formed: high-lying loops filled with hot plasma (131 and 94 Å) and low-lying loops filled with cold and dense plasma (171 Å). Thus, at 16:13:26 UTC, the plasma density at the looptops in the loop interaction region may have been sufficiently high ($> 10^{10} \,\mathrm{cm}^{-3}$). A further increase in plasma density may result from material accumulation due to chromospheric evaporation, which is triggered when accelerated electrons heat the chromospheric plasma [23]. However, the plasma evaporation process is relatively slow compared to the duration of individual spikes. In addition to the high plasma density, the generation of HXR spikes at the looptop also requires the accumulation of accelerated electrons. Therefore, the question arises as to where the electron acceleration and injection into the closed magnetic loop system are localized. According to the standard solar flare model [24], electron acceleration occurs in the cusp region of the corona. The subsequent injection into the looptops of closed magnetic loops occurs at a significantly lower altitude, although still within the corona. Magnetic mirroring from strong-field regions and the possible backscattering of accelerated electrons from the electric fields of various turbulence modes contribute to their accumulation in the looptop region of flare loops [25]. Such an accumulation of electrons at the looptop can compensate for their losses due to precipitation into the loop footpoints and provide a sufficient density to generate the observed HXR spikes.

In addition to particle accumulation at the looptop, the timescale of electron acceleration is also a key fac-Generation of the observed HXR spikes at the F times requires electron acceleration up to the energies of $\sim 100\,\mathrm{keV}$ for a time that is comparable to or less than Various mechanisms can accelerate the spike duration. electrons to high energies of up to tens of MeV within millisecond timescales. For example, in a state of selforganized criticality, such acceleration can occur through an avalanche of small magnetic reconnection events in the coronal magnetic field [26]. However, the issue of particle acceleration must be addressed separately. In this study, we limited our scope to estimating the strength of the induced electric field, which occurs during a change in the magnetic field. According to Faraday's law, the equation for electromagnetic induction is as follows:

$$\oint \mathbf{E} \, dl = -\frac{1}{c} \, \int \left(\frac{\partial \mathbf{B}}{\partial t} \, dS \right),$$

where E is the electric field, B is the magnetic field induction, the line integral is taken along the closed contour L, the surface integral is taken over any surface S bounded by

S, and c is the speed of light. We estimated the magnitude of the rotational electric field E and compared it with the Dreicer field [27]. Using EUV images, we chose a circular cross-section as the contour with a radius of R, comparable to the spatial scale of the magnetic field variation during the flare's impulsive phase, and the boundary L corresponds to the circumference of the contour S. We evaluate the circulation of the vector **E** as $E2\pi R$, while the derivative of the magnetic field we evaluate as $(1/c)(\partial B/\partial t)\pi R^2$. The value of the field E is determined by the rate of variation of induction of the magnetic field B and by the radius of the circular contour R, $E = (\partial B/\partial t)R/2c$, where cthe speed of light. First, to estimate the Dreicer electric field, we will use the definition $E_{\rm Dr} = \lambda e/r_{\rm D}^2$, where λ is the Coulomb logarithm, we will take it to be equal to 20, e is the electron charge, and r_D is the electron Debye radius. Since the magnetic field varies in the coronal region, we assume that the value of the temperature is $10^6 \, \mathrm{K}$ and the density is $10^{10} \,\mathrm{cm}^{-3}$. In this case $r_{\mathrm{D}} = 0.07 \,\mathrm{cm}$, while $E_{\rm Dr} = 2 \cdot 10^{-6}$ statV/cm. For the rate of variation of the magnetic field $\sim 1\,\text{G/s}$ [28] within the contour of the radius 10^{8-9} cm, we obtain an estimate of the value of the induction electric field $E \simeq (10^{-3} - 10^{-2}) \, \text{statV/cm}$. As shown in the paper [29], the electron acceleration in the super-Dreicer fields to the energies of 100 keV and higher can occur in current sheets of a small length of $\sim 100\,\mathrm{m}$. At the same time, the impulsive bursty reconnection mode in the current sheet is realized as a result of tearing-mode instability at sub-second times [30].

We note that the classic formula for the Dreicer field used within the framework of the simple models is rather conditional. As shown by more detailed calculations [31], the actual critical field can differ from the formal expression by up to five times, especially, when considering dynamic friction and interactions between the accelerated and thermal electrons. Therefore, any use of the traditional definition must explicitly state its limitations, particularly the assumptions of a stationary particle distribution and the absence of turbulence. In the context of realistic solar flare conditions, a correction to the classical formula is necessary for detailed modeling of acceleration processes.

We provide an estimate of the typical loop length and maximum potential for electron acceleration under the field of the order of the Dreicer field, based on the observed delays Δt between the high- and low-energy channels of X-ray radiation and using the standard TOF method [32].

We assume that $\Delta t_{ij} \approx 77\,\mathrm{ms}$ — the difference of radiation arrival times with the energies $E_i \approx 13.5\,\mathrm{keV}$ and $E_j \approx 66.6\,\mathrm{keV}$ (Fig. 7). The electron velocities of the corresponding energies are $v_i = 6.9 \cdot 10^9\,\mathrm{cm/s}$ and $v_j = 15.4 \cdot 10^9\,\mathrm{cm/s}$. Then, using the formula $L_{\mathrm{TOF}} = \Delta t_{ij} (1/v_i - 1/v_j)^{-1}$, we obtain the estimate $L_{1,3} \approx 10^9\,\mathrm{cm}$. We emphasize that this value provides only a rough estimate of the loop half-length (or effective path length) for sub-second pulses. For the coronal plasma with $n \sim 10^{10}\,\mathrm{cm}^{-3}$ and $T \sim 10^6\,\mathrm{K}$, the value of the Dreicer field E_{Dr} , as shown above, can reach $10^{-6}\,\mathrm{statV/cm}$, and

taking into account clarification [31] $E_{\rm D}\approx 0.2E_{\rm Dr}$. In our conditions we take that $E_{\rm Dr}\approx 2\cdot 10^{-6}~{\rm statV/cm}$. Then, the total potential when passing the length $L_{\rm TOF}\sim 10^9~{\rm cm}$ is: $\Phi_{\rm max}=E_{\rm Dr}\,L_{\rm TOF}\approx 2\cdot 10^{-6}~{\rm statV/cm}\cdot 10^9~{\rm cm}$. Converting the statvolts into volts (1 statV $\approx 300~{\rm V}$), we obtain that $\Phi_{\rm max}\approx 6\cdot 10^5~{\rm V}\equiv 600~{\rm keV}$. If it is assumed that the real $E_{\rm Dr}$ can be less than the said approximately in 4–5 times [31], then the maximum "threshold" of energy falls to the values about 120–150 keV.

Thus, for the loop of the length $\sim 10^9$ cm, within the framework of the "classic" sub-Dreicer model (with the homogeneous plasma and stationary configuration of the field) the limit electron energy turns out to be about $100-600\,\mathrm{keV}$. In practice, however, acceleration in an actual flare can occur in much smaller and highly inhomogeneous regions (e.g., in super-Dreicer fields, through turbulent pumping, etc.). Therefore, this estimate serves only as a guideline, demonstrating that a model with a sub-Dreicer electric field is unlikely to account for particle acceleration to several hundred keV and higher energies without considering additional mechanisms or local field enhancements. We note that in this study, we considered electron energies below $100\,\mathrm{keV}$.

Conclusion

This study investigated the spatial distribution of the sources of subsecond HXR spikes during solar flares. The primary challenge in studying spikes is their low intensity and short durations. While it was traditionally believed that accelerated electrons generate spikes in dense chromospheric plasma, modeling and observations of behind-the-limb flares suggest that spikes can also form in coronal looptops.

As a case study, we analyzed the M1.3 class behind-the-limb flare SOL2017-07-03, in which HXR spikes were detected. Analysis of the ultraviolet images localized the emission sources at the looptop of a low-lying loop structure. The centroids of the RHESSI X-ray images within the range $11-26\,\mathrm{keV}$ were located at the looptop of the low magnetic loop. During the rise phase of the HXR emission, the Fermi GBM spectrometer registered individual spikes with a duration of $300-700\,\mathrm{ms}$ in the 11-26, 26-50, and $50-100\,\mathrm{keV}$ energy ranges. Spike profiles are symmetric, in contrast to the profiles of elementary bursts with durations of $> 1\,\mathrm{s}$.

We propose a method for detecting spikes in HXR time series based on an analysis of the standard deviation and multipoint spike profile across different energy ranges.

Thus, we have shown that HXR spikes can be generated not only at the footpoints but also at the looptops or in the lower corona at the transition region boundary, where the plasma density is lower. These results broaden our understanding of HXR emission generation during solar flares and highlight the importance of further investigating behind-the-limb events to study particle acceleration mechanisms in

the corona and probe plasma parameters (temperature and density) at flare looptops.

Funding

The work of Yu.E. Charikov (problem formulation, manuscript writing) and E.M. Sklyarova (data processing) was supported by the State Program FFUG-2024-0002. The work of A.N. Shabalin (manuscript writing, RHESSI and SDO data processing) was supported by the Russian Science Foundation grant No. 20-72-10158.

Conflict of interest

The authors declare that they have no conflict of interest.

References

- A.L. Kiplinger, B.R. Dennis, K.J. Frost., L.E. Orwig, A.G. Emslie. Astrophys. J., 265, 99 (1983). DOI: 10.1086/183966
- [2] A.L. Kiplinger, B.R. Dennis, K.J. Frost, L.E. Orwig. Astrophys. J., 287, 105 (1984). DOI: 10.1086/184408
- [3] G.J. Fishman, C.A. Meegan, R.B. Wilson, W.S. Paciesas, G.N. Pendleton. NASA Conf. Publ., 3137, 26 (1992).
- [4] L.E. Orwig, K.J. Frost, B.R. Dennis. Sol. Phys., 65, 25 (1980). DOI: 10.1007/BF00151382
- [5] R.L. Aptekar, D.D. Frederiks, S.V. Golenetskii, V.N. Ilynskii, E.P. Mazets, V.N. Panov, Z.J. Sokolova, M.M. Terekhov, L.O. Sheshin, T.L. Cline, D.E. Stilwell. Space Sci. Rev., 71, 265 (1995). DOI: 10.1007/BF00751332
- [6] C. Meegan, G. Lichti, P.N. Bhat, E. Bissaldi, M.S. Briggs, V. Connaughton, R. Diehl, G. Fishman, J. Greiner, A.S. Hoover, A.J. Van Der Horst, A. Von Kienlin, R.M. Kippen, C. Kouveliotou, S. McBreen, W.S. Paciesas, R. Preece, H. Steinle, M.S. Wallace, R.B. Wilson, C. Wilson-Hodge. Astrophys. J., 702 (1), 791 (2009). DOI: 10.1088/0004-637X/702/1/791
- Y. Ogawara, T. Takano, T. Kato, T. Kosugi, S. Tsuneta,
 T. Watanabe, I. Kondo, Y. Uchida. Sol. Phys., 136 (1), 1 (1991). DOI: 10.1007/BF00151692
- [8] R.P. Lin, B.R. Dennis, G.J. Hurford, D.M. Smith, A. Zehnder, P.R. Harvey, D.W. Curtis, D. Pankow, P. Turin, M. Bester, A. Csillaghy, M. Lewis, N. Madden, H.F. van Beek, M. Appleby, T. Raudorf, J. McTiernan, R. Ramaty, E. Schmahl, R. Schwartz, S. Krucker, R. Abiad, T. Quinn, P. Berg, M. Hashii, R. Sterling, R. Jackson, R. Pratt, R.D. Campbell, D. Malone, D. Landis, C.P. Barrington-Leigh, S. Slassi-Sennou, C. Cork, D. Clark, D. Amato, L. Orwig, R. Boyle, I.S. Banks, K. Shirey, A.K. Tolbert, D. Zarro, F. Snow, K. Thomsen, R. Henneck, A. Mchedlishvili, P. Ming, M. Fivian, John Jordan, Richard Wanner, Jerry Crubb, J. Preble, M. Matranga, A. Benz, H. Hudson, R.C. Canfield, G.D. Holman, C. Crannell, T. Kosugi, A.G. Emslie, N. Vilmer, J.C. Brown, C. Johns-Krull, M. Aschwanden, T. Metcalf, A. Conway. Sol. Phys., 210, 3 (2002). DOI: 10.1023/A:1022428818870
- [9] T. Knuth, L. Glesener. Astrophys. J., 903 (1), 63 (2020). DOI: 10.3847/1538-4357/abb779
- [10] K. Arzner. Sol. Phys., **210**, 213 (2002). DOI: 10.1023/A:1022417825577
- [11] J. Qiu, J.X. Cheng, G.J. Hurford, Y. Xu, H. Wang. Astron. Astrophys., 547, A72 (2012). DOI: 10.1051/0004-6361/201118609

- [12] J.X. Cheng, J. Qiu, M.D. Ding. H. Wang. Astron. Astrophys., 547, A73 (2012). DOI: 10.1051/0004-6361/201118608
- [13] Electronic source. The Konus-Wind catalog of BTL flares. Available at: www.ioffe.ru/LEA/kw/wm/btl/index.html (retrieved on May 14, 2024)
- [14] W.D. Pesnell, B.J. Thompson, P.C. Chamberlin. Solar Phys., 275, 3 (2012). DOI: 10.1007/s11207-011-9841-3
- [15] T. Wiegelmann, G.J.D. Petrie, P. Riley. Space Sci. Rev., 210, 249 (2017). DOI: 10.1007/S11214-015-0178-3
- [16] B.R. Dennis, M.A. Duval-Poo, M. Piana, A.R. Inglis, E.A. Gordon, J. Guo, Y. Xu. Astrophys. J., 867, 82 (2018). DOI: 10.3847/1538-4357/aae0f5
- [17] A.N. Shabalin, E.P. Ovchinnikova, Y.E. Charikov. Astrophys. J., 954, 58 (2023). DOI: 10.3847/1538-4357/acea5e
- Y.E. Charikov, A.N. Shabalin, E.P. Ovchinnikova. Geomagn. Aeron., 59 (7), 870 (2019).
 DOI: 10.1134/S0016793219070107
- [19] P. Zhang, W. Wang, Y. Su, S. Zhang, L. Song, F. Lu, S. Zhang. Res. Astron. Astrophys., 22 (5), 055006 (2022).
 DOI: 10.1088/1674-4527/AC5958
- [20] M.J. Aschwanden, R. Schwartz. Astrophys. J., 455, 699 (1995). DOI: 10.1086/176617
- [21] Yu.T. Tsap, I.N. Myagkova, Yu.G. Kopylova, G.G. Motorina, A.V. Bogomolov, T.B. Gol'dvarg, M.I. Panasyuk, S.I. Svertilov, V.V. Bogomolov, I.V. Yashin, V.L. Petrov. Cosmic Research, 56 (6), 420 (2018). DOI: 10.1134/S0010952518060096
- [22] A.V. Stepanov, V.V. Zaitsev. *Magnitosfery aktivnykh oblastei Solntsa i zvezd* (Fizmatlit, M., 2018) (in Russian).
- [23] W. Liu, V. Petrosian, J.T. Mariska. Astrophys. J., 702 (2), 1553 (2009). DOI: 10.1088/0004-637X/702/2/1553
- [24] K. Shibata, T. Magara. Living Rev. Sol. Phys., 8, 6 (2011). DOI: 10.12942/LRSP-2011-6
- [25] Y.E. Charikov, A.N. Shabalin. Tech. Phys., 66 (8), 1092 (2021). DOI: 10.1134/S1063784221080053
- [26] E.T. Lu., R.J. Hamilton. Astrophys. J. Lett., 380, L89 (1991). DOI: 10.1086/186180
- [27] H. Dreicer. Phys. Rev., 115 (2), 238 (1959).DOI: 10.1103/PhysRev.115.238
- [28] G.D. Fleishman, D.E. Gary, B. Chen, N. Kuroda, S. Yu, G.M. Nita. Science, 367 (6475), 278 (2020). DOI: 10.1126/science.aax6874
- [29] Y.E. Litvinenko. Astrophys. J., 462, 997 (1996). DOI: 10.1086/177213
- [30] B. Kliem, M. Karlicky, A.O. Benz. Astron. Astrophys., 360 (2), 715 (2000). DOI: 10.48550/arXiv.astro-ph/0006324
- [31] Y.T. Tsap, A.V. Stepanov, Y.G. Kopylova. Res. Astronom. Astrophys., 24 (2), 025015 (2024).
 DOI: 10.1088/1674-4527/AD1BD5
- [32] M.J. Aschwanden. *Physics of the Solar Corona* (Springer, Berlin, Heidelberg, 2006), DOI: 10.1007/3-540-30766-4

Translated by M.Shevelev